INSTITUTE OF PHYSICS PUBLISHING NANOTECHNOLOGY
Nanotechnology **15** (2004) S122–S125 PII: S0957-4484(04)70116-6

Fabrication of arrays of $SrZrO_3$ nanowires by pulsed laser deposition

S Karthäuser[1], **E Vasco, R Dittmann and R Waser**

Institut für Festkörperforschung and Centre of Nanoelectronic Systems for Information Technology, Forschungszentrum Jülich, D-52425 Jülich, Germany

E-mail: s.karthaeuser@fz-juelich.de

Received 24 September 2003, in final form 4 December 2003
Published 23 January 2004
Online at stacks.iop.org/Nano/15/S122 (DOI: 10.1088/0957-4484/15/4/002)

Abstract
$SrZrO_3$ thin films grown by pulsed laser deposition on $SrRuO_3$-buffered $SrTiO_3$ substrates have been investigated by means of x-ray diffraction, atomic force microscopy and Rutherford backscattering spectroscopy. The compressive stress originated in the coherent $SrZrO_3/SrRuO_3$ interface due to the lattice mismatch ($\approx -4.5\%$) forces epitaxial $SrZrO_3$ to grow in a three-dimensional habit. So-deposited $SrZrO_3$ is used to fabricate nanoarrays of dielectric wires from a nanopatterned $SrRuO_3$ surface. The influence of the geometric shadowing effect produced by the non-perpendicular incidence of the ablated particles on the $SrZrO_3$ growth habit is discussed.

1. Introduction

In the last few decades oxide thin films based on perovskites have attracted increasing attention as novel electrochemical devices. $SrZrO_3$ with a good chemical and mechanical stability is an especially promising candidate for use in solid oxide fuel cells and hydrogen sensors due to its proton conductivity at elevated temperatures [1, 2]. Besides this, several characteristics such as high dielectric constant ($\sim$60.0) and high breakdown strength (400 kV cm^{-1}) [3] make $SrZrO_3$ particularly suitable for high voltage and high reliability capacitive applications. In addition $SrZrO_3$ thin films with transition metal doping are possible candidates for use in non-volatile random access memories [4, 5]. These films epitaxially stacked in a metal–insulator–metal device have been reported to show a reproducible bistable switching between a low and a high impedance state or even a multilevel switching which offers a large potential for novel memory devices.

Involved in the effort to scale up memory densities to the Gbit region, memory cell sizes in the nanometre range are required. An attractive fabrication route for such nanostructures is provided by the self-organized deposition techniques, which take advantage of periodic arrangements of kinks and steps as well as stress-induced surface modulations. Thus, a combination of lattice-mismatched materials has been exploited in the semiconductor growth to form 2D arrays of nanometre-sized islands with narrow size distributions [6]. Here, we adopt this nanopatterning principle to fabricate nanostructures of perovskite oxides. The ability of the heteroepitaxial $SrZrO_3/SrRuO_3/SrTiO_3$ system to self-organize into arrays of ordered nanostructures driven by a high degree of lattice mismatch is investigated. $SrRuO_3$ is a ternary transition metal oxide suitable for use as an electrode due to its good electrical conductivity. The nominal lattice mismatch between the orthorhombic unit cell of $SrRuO_3$ (SRO) ($a_o = 0.5567$ nm, $b_o = 0.5535$ nm, $c_o = 0.7845$ nm), which can be described as a pseudocubic unit cell ($a_c = 0.393$ nm, $\alpha = \beta = 90°$ and $\gamma = 89.67°$), and the cubic $SrTiO_3$ (STO) cell ($a_c = 0.3905$ nm) is only 0.64% supporting an epitaxial growth [7]. On the other hand, $SrZrO_3$ (SZO) has an orthorhombic structure ($a_o = 0.5814$ nm, $b_o = 0.5792$ nm and $c_o = 0.8196$ nm) resulting in a SZO/SRO lattice mismatch between -4.3 and -4.6%. The effect of this high degree of lattice mismatch ($\sim$strain) upon the epitaxial growth process is studied in this work.

2. Experimental details

The SZO films were grown by pulsed laser deposition (PLD) on epitaxial SRO/STO by using a KrF excimer laser ($\lambda = 248$ nm) that emits 16 ns pulses with an energy density of $J = 5$ J cm^{-2} at a frequency of 10 Hz. The substrates, which were prepared

[1] Author to whom any correspondence should be addressed.

by the pulsed laser deposition of $SrRuO_3$ on chemically treated $SrTiO_3$ substrates [7][2], were placed opposite to the target at a distance of 60 mm and heated within the temperature range of $650 \leqslant T_s/°C \leqslant 800$. The SZO growth was performed in a high vacuum chamber (base pressure: 1×10^{-5} mbar) in the presence of an oxygen dynamic pressure of $P_{O_2} = 0.5$ mbar (except during the shadowing experiments in which $P_{O_2} = 10^{-4}$ mbar was also used). The average deposition rate was about 1.8 ± 0.3 Å s^{-1}.

The crystallinity and orientation of the SZO films were analysed by means of x-ray diffraction using a four-circle X'Pert Philips diffractometer in $\theta/2\theta$ and ϕ-scan modes with Cu Kα radiation. The SZO film morphology was studied by atomic force microscopy (AFM) in non-contact mode by means of a commercial surface image system (SIS) set-up equipped with a Si cantilever with a nominal tip radius of 10 nm and a spring constant of $k = 40$ N m^{-1}. Additionally AFM measurements with conductive Pt/Ir coated silicon tips were carried out employing a JEOL JSPM-4210 in contact mode. The RBS data were collected at a Tandetron accelerator with a 1.4 MeV He^{2+} beam. The random RBS spectrum was simulated using the RUMP code [8].

3. Results

Figure 1 shows a typical SZO/SRO/STO $\theta/2\theta$ spectrum measured within the $2\theta = 15°$–$55°$ range. With the exception of the substrate and buffer layer peaks (00l STO and hh0/00l SRO, respectively) only the hh0/00l SZO diffractions are observed, which suggests that the SZO films are at least strongly textured. The scant separation between the hh0 SZO and 00l SZO diffractions ($<0.05°$) impedes distinguishing between the contributions. The ϕ-scan analysis displayed in figure 2 completes the above picture demonstrating that SZO grows epitaxially on SRO/STO exhibiting between two and four coexistent out-of-plane orientations (domains):

- domain A and/or A*: [110]SZO ∥ [110]SRO and/or [001]SRO ∥ [001]STO
- domain B and/or B*: [001]SZO ∥ [110]SRO and/or [001]SRO ∥ [001]STO

each of them formed by two in-plane epitaxial arrangements:

- domain A and/or A*: [001]SZO ∥ [100]STO and [001]SZO ∥ [010]STO
- domain A and/or A*: [110]SZO ∥ [100]STO and [110]SZO ∥ [010]STO.

The small differences between the strains originated by the epitaxial arrangements (range between −4.3 and −4.6%) prevent us from discarding the possibility of the presence of some domains. In any case, such relatively high compressive strains are of the order of those (∼5%) induced by the SZO direct deposition on (001)STO.

The typical SZO/SRO/STO surface morphology imaged by AFM is shown in figure 3. After deposition of 6 nm SZO on the vicinal departing surface, the SRO/STO flat terraces

[2] Commercially available STO substrates were chemically treated with a NH_4F buffered HF solution in order to prepare a TiO_2-terminated regular vicinal surface, which promotes the ordered growth of the $SrRuO_3$ buffer layer. Details of the chemical treatment used are provided elsewhere [14].

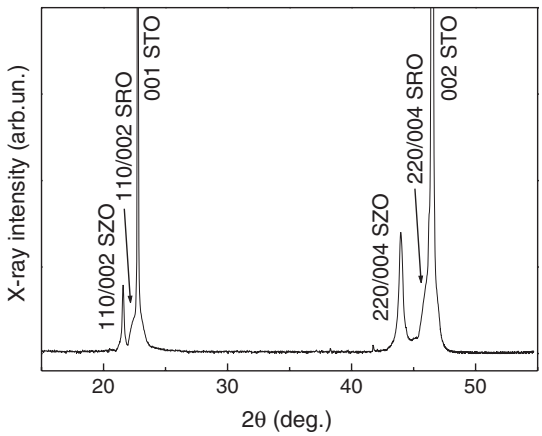

Figure 1. The $\theta/2\theta$ x-ray spectrum of a 30 nm $SrZrO_3$/30 nm$SrRuO_3$/$SrTiO_3$ heterostructure.

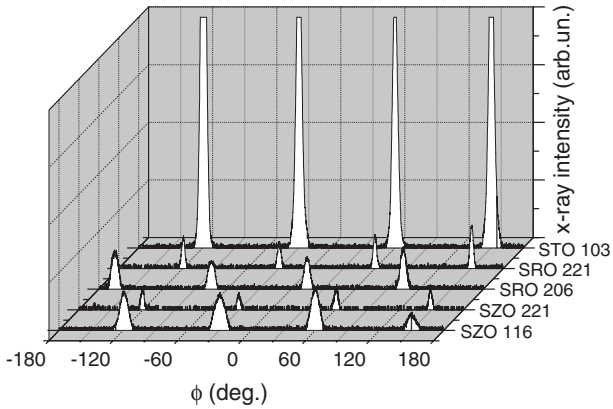

Figure 2. ϕ-scan x-ray spectra of a 33 nm $SrZrO_3$/33 nm $SrRuO_3$/$SrTiO_3$ heterostructure. The spectra were obtained by assuming the following out-of-plane orientations: (SRO 221) [110]$SrRrO_3$ ∥ [001]$SrTiO_3$, (SRO 206) [001]$SrRrO_3$ ∥ [001] $SrTiO_3$, (SZO 221) [110]$SrZrO_3$ ∥ [001]$SrTiO_3$ and (SZO 116) [001]$SrZrO_3$ ∥ [001]$SrTiO_3$.

(figure 3(a)) appear decorated with 3D SZO protrusions (figure 3(b)). This behaviour suggests that SZO starts growing in a 3D habit at very early stages. Details of these surface features are displayed in figure 4. The regular circular protrusions extend up to 100 nm exhibiting smooth surfaces characterized by moderate slopes (e.g. slope ≈1 nm/30 nm and 2 nm/30 nm for the 6 nm SZO/33 nm SRO/STO and 33 nm SZO/33 nm SRO/STO heterostructures, respectively). These observations point to the presence of a 3D growth habit that evolves as a function of the strain energy according to a Volmer–Weber or Stranski–Krastanov growth mode. In the case of Volmer–Weber growth, the protrusions would coalesce into larger features giving rise to a compact film as the deposition progresses, while in the Stranski–Krastanov case the protrusions are built at the surface of the growing SZO film to relieve the increasing misfit-induced stress.

The morphological evolution of the SZO film surface has been studied within the framework of the dynamic scaling theory [9]. The mean square deviation of the sample surface (roughness), $\sigma_{SZO/SRO/STO}$, was determined from the 5×5 μm^2 imaged areas. The SRO/STO contribution to the sample roughness was systematically removed as: $\sigma_{SZO} =$

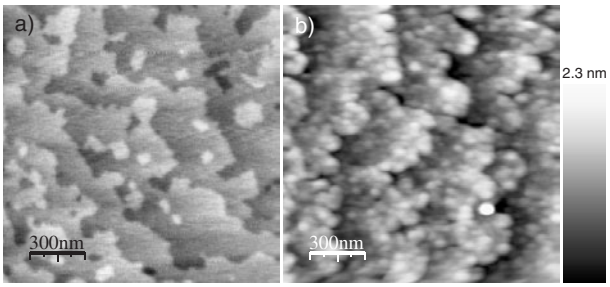

Figure 3. AFM images of: (a) a departing vicinal surface (33 nm $SrRuO_3/SrTiO_3$), (b) a surface of a 6 nm thick $SrZrO_3$ film.

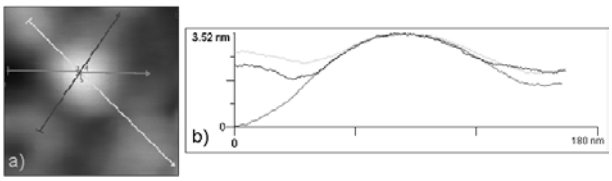

Figure 4. (a) Topographic details of a $SrZrO_3$ protrusion. (b) Profiles taken in three representative directions revealing the protrusion round symmetry. The scanned area is 200×200 nm^2.

$\sqrt{\sigma^2_{\mathrm{SZO/SRO/STO}} - \sigma^2_{\mathrm{SRO/STO}}}$ in order to properly analyse the evolution of the SZO film roughness, σ_{ZO}. The dependence of the film roughness on the deposition time, $\sigma_{\mathrm{SZO}}(t)$, is shown in figure 5. σ_{SZO} scales with t as: $\sigma_{\mathrm{SZO}} \sim t^{\beta}$, $\beta = 0.93 \pm 0.95$ being the growth exponent. The high β value obtained (>0.5) indicates the presence of an unstable 3D growth [9], in which the surface lateral relaxation is inhibited. The dependence of σ_{SZO} on the deposition temperature, T, for 30 nm thick SZO films is also included in figure 5 as an Arrhenius plot. The quasi-constant behaviour of $\sigma_{\mathrm{SZO}}(T)$ points to two exclusive possibilities: (i) the superficial diffusion is not activated within the 650–800 °C range that would imply hopping energy barriers as high as 2.6 eV (considering a deposition rate and a pre-exponential factor of 1 ML s^{-1} and 10^{12} s^{-1}, respectively); or (ii) the surface mass transport takes place preferentially towards the nucleation centres, which coarsen in a 3D way.

In this latter case, $\sigma_{\mathrm{SZO}}(T) \approx$ constant points to a post-nucleation roughness saturation regime characterized by diffusion lengths larger than the distance between centres. AFM images exhibiting how the SZO growth proceeds through the formation of isotropic 3D protrusions (figure 4) support the second above-suggested hypothesis. In addition, the thermal instability of 2D compact SZO films and their evolution to unconnected 3D single-crystalline grains has been previously observed on STO(001) [10]. Thus, the massive aggregation to the 3D centres becomes energetically more favourable than the layer-by-layer growth due probably to the high formation energy of the highly stressed SZO/SRO interface.

Since the growth exponent obtained is close to that predicted theoretically [11] ($\beta = 1$) for the geometric shadowing effect, the angular distribution of the ablated particles has been studied in detail. This analysis has been performed by means of the edge profiles of areas artificially shadowed by a stainless steel mask localized 0.5 mm away from the substrate surface in SZO films deposited at room temperature in $P_{O_2} = 10^{-4}$ and 0.5 mbar. The low deposition temperatures prevent phenomena such as the edge diffusion

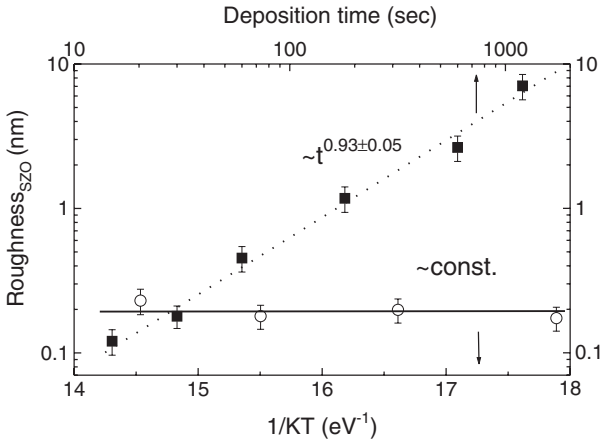

Figure 5. (■) Deposition time dependences at 750 °C and (○) temperature dependences (at 30 s deposition time) of the roughness of $SrZrO_3$ films deposited on 33 nm $SrRuO_3/SrTiO_3$. The symbols represent the data points while the dotted lines correspond to the indicated fittings. An averaged $SrRuO_3/SrTiO_3$ roughness contribution of $\sigma_{\mathrm{SRO/STO}} = 0.21$ nm was assumed for all samples.

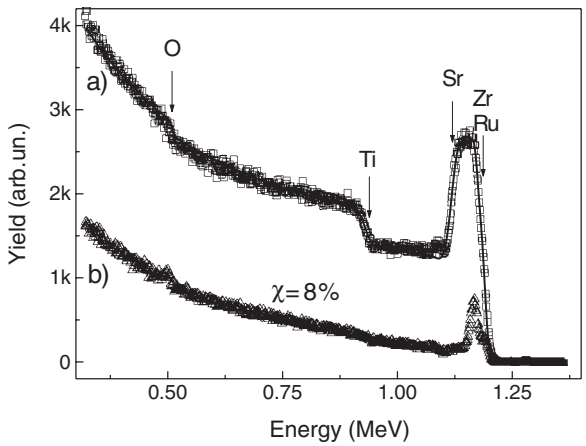

Figure 6. RBS random (a) and channelling (b) spectra of a 12 nm $SrZrO_3$/33 nm$SrRuO_3/SrTiO_3$ heterostructure. The symbols represent the experimental data points while the solid curve corresponds to the simulated spectrum. The backscattering energy corresponding to each element on top of its layer is indicated.

and the multiple reflections of re-emitted particles on the back of the mask. While the dispersion average angle estimated for the films deposited at $P_{O_2} = 10^{-4}$, $\langle\theta\rangle = 3°$, is included in the assumed beam width ($\leqslant 4.7°$) considering the front of the evaporated particle wave as flat; the dispersion average angle rises significantly as the oxygen pressure increases. Thus, an angular distribution of evaporated particles of $\approx \cos^{23\pm3}(\theta)$ with a $\langle\theta\rangle = 28° \pm 2°$ has been estimated at $P_{O_2} = 0.5$ mbar. Afterwards, an influence of the geometric shadowing effect, which is inherent to the vapour phase deposition under high oxygen pressures, on the SZO morphology evolution cannot be ruled out. In fact, the relevance of this phenomenon has been previously reported for other perovskite oxides deposited by PLD at comparable oxygen pressures [12]. However, the shadowing effect is not able to provide a reliable explanation for the $\sigma_{\mathrm{SZO}}(T)$ dependence shown in figure 5, because a $\sigma_{\mathrm{SZO}}(T) \neq$ constant is expected as the thermally activated surface diffusion counterbalances the shadowing influence.

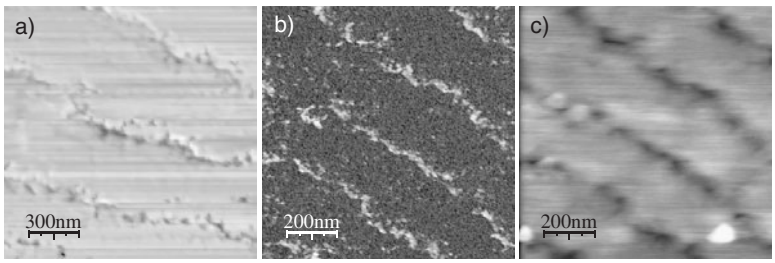

Figure 7. A conducting AFM image of rippled $SrRuO_3/SrTiO_3$ (a) and conducting (b) and topographic (c) AFM images of 6 nm $SrZrO_3$ deposited on rippled $SrRuO_3/SrTiO_3$.

Therefore, the 3D growth habit characteristic of SZO films deposited on SRO/STO is not a direct consequence of the shadowing effect, which becomes relevant on surface areas characterized by large local slopes.

Special attention has been paid to the study of the chemical composition of the deposited films due to the early reports that point to a chemical miscibility between SZO and STO [10]. The simulated random RBS spectrum demonstrates that all layers of the heterostructure are stoichiometric and their interfaces abrupt without evidence of massive interdiffusion processes or formation of solid solutions. This behaviour suggests that even at low pressure the formation temperature of such solid solutions is higher than those used here[3]. The channelling RBS spectrum, also included in figure 6, reveals the high crystalline quality of the SZO/SRO/SRO heterostructure, such that its minimum yield ($\chi = 8\%$) is comparable to that obtained in epitaxial SZO/STO [13].

Additional insights into the growth process of SZO on SRO buffered STO substrates are obtained from AFM measurements performed with a conducting tip which allows to identify SZO during its first growth stages (prior to the film completion regime) on the basis of the difference between the electrical conductivities of SZO and SRO. Employing a photochemically treated STO substrate [14], rippled SRO buffer layers can be formed which are used as templates for the ordered growth of SZO. In figure 7 the conducting (b) and topographic (c) images corresponding to the same area of a 6 nm SZO film deposited on highly conductive rippled SRO/STO (figure 7(a)) are shown. Correlating the three images, the SZO nanowire array (black areas in figure 7(b)) grown on the ripple tops and separated by deep and narrow boundaries that extend down to the conductive buffer layer (light area) can be recognized. Obviously the light conductive areas in figure 7(b) correspond to the wire boundaries in 7(c) that coincide with the SRO inter-ripple boundaries. The formation of these non-conductive SZO wires on the SRO ripple axis is supported by the shadowing effect that becomes relevant in the inter-ripple boundaries assisted by the SZO tendency to a 3D growth mode.

4. Conclusion

The here-presented experimental study demonstrates that thin films of $SrZrO_3$ can be epitaxially and stoichiometric grown on a $SrRuO_3$ buffered $SrTiO_3$ substrates despite the high lattice mismatch of about -4.5% between $SrZrO_3$ and $SrRuO_3$. Originating from this lattice mismatch and influenced by the geometric shadowing effect, $SrZrO_3$ presents a 3D growth habit from the early stages, which can be conveniently used on nanopatterned surfaces to fabricate arrays of non-conductive wires.

Acknowledgment

This work was supported by Deutsche Bundesministerium für Bildung und Forschung under Grant No 13N8361.

References

[1] Shin S, Huang H, Ishigame M and Iwahara H 1990 *Solid State Ion.* **40/41** 910
[2] Higuchi T, Tsukamoto T, Sata N, Hiramoto K, Ishigame M and Shin S 2001 *Japan. J. Appl. Phys.* 1 **40** 4162
[3] Shende R, Krueger D, Rossetti G and Lombardo S 2001 *J. Am. Ceram. Soc.* **84** 1648
[4] Beck A, Bednorz J, Gerber Ch, Rossel C and Widmer D 2000 *Appl. Phys. Lett.* **77** 139
[5] Rossel C, Meijer G, Brémaud D and Widmer D 2001 *J. Appl. Phys.* **90** 2892
[6] Moriarty P 2001 *Rep. Prog. Phys.* **64** 297–381
[7] Choi J, Eom C, Rijnders G, Rogalla H and Blank D 2001 *Appl. Phys. Lett.* **79** 1447
[8] Doolittle L R 1984 *Nucl. Instrum. Methods* B **9** 334
[9] Barabási A L and Stanley H E 1995 *Fractal Concepts in Surface Growth* (New York: Cambridge University Press)
[10] Langjahr P A, Wagner T, Rühle M and Lange F F 1999 *J. Mater. Res.* **14** 2945
[11] Roland C and Guo H 1991 *Phys. Rev. Lett.* **66** 2104
[12] Vasco E, Polop C and Ocal C 2003 *Eur. J. Phys.* B **35** 49
[13] Beckers L, Sanchez F, Schubert J, Zander W and Buchal C 1996 *J. Appl. Phys.* **79** 3337
[14] Karthäuser S, Szot K and Waser R, in preparation

[3] Langjahr *et al* [10] reported a formation temperature at room pressure for the $SrZrO_3$–$SrTiO_3$ solution as high as 1150 °C.